Original Article

Institution of MECHANICAL ENGINEERS
Journal of POWER AND ENERGY

Proc IMechE Part A:
J Power and Energy
2017, Vol. 231(2) 87–101

DOI: 10.1177/0957650916677428
journals.sagepub.com/home/pia
SAGE

Experimental and numerical investigations on the aerodynamic performance of a pivoted Savonius wind turbine

M Amiri, AR Teymourtash and M Kahrom

Abstract

Savonius turbines have been the subject of various wind energy projects due to their good starting characteristics, easy installation, and independency of wind direction. However, the Savonius rotor suffers from low aerodynamic performance, which is mainly due to the adverse torque of the returning blade. A recently introduced design suggests using pivoted blades for the rotor to eliminate the negative torque of the returning blade. In this study, the aerodynamic performance of the newly proposed turbine has been investigated experimentally and numerically. The experimental measurements are performed in a subsonic open-jet type wind tunnel facility. The numerical simulations are performed using ANSYS-Fluent commercial software, by making use of the multiple reference frame model. The effects of the number of blades (3-, 4-, and 6-bladed) on the torque and power coefficients are examined in details, at several Reynolds numbers. Results show that the new rotor has no negative torque in one complete revolution and that the 3-bladed rotor has the best aerodynamic performance, in a manner that, it reaches a maximum power coefficient of 0.21 at $TSR = 0.5$. Although increasing the number of blades decreases the output torque oscillations, it also decreases the average power coefficient of the rotor. Results show that Reynolds number does not have a significant effect on the average power coefficient of the rotor in the studied range of $7.7 \times 10^4 \leqslant Re \leqslant 1.2 \times 10^5$.

Keywords

Pivoted Savonius, aerodynamic performance, multiple reference frame, vertical axis

Date received: 24 September 2016; accepted: 6 October 2016

Introduction

Wind energy is one of the best candidates for green economical energy production, among the various available renewable energy sources. Wind turbines, a main element in the wind energy harnessing, might be classified into two main categories based on the rotation axis alignment:[1] vertical axis wind turbine (VAWT) and horizontal axis wind turbine (HAWT). Savonius rotor is one of the simplest designs of the VAWTs, a drag-type turbine that consists of two or more semicircular blades. Despite its low efficiency, the Savonius rotor takes advantage of several privileges such as, good starting characteristics, easy installation, and independency of wind direction (omnidirectional).[2] These benefits have motivated numerous researches to modify the aerodynamic performance of the Savonius-type rotors.

Fujisawa[3] experimentally investigated the aerodynamic performance and the flow fields of Savonius rotors at various overlap ratios, where the best power coefficient occurred at an overlap ratio of 0.15. Kianifar and Anbarsooz[4] studied the effects of blade curve and overlap ratio on the performance of Savonius rotors. The results showed that the semicircular blades with an overlap ratio of 0.2 had the best power performance. Alexander and Holownia[5] tested the effects of end plates and revealed that a higher rotor performance can be obtained using end plates for the Savonius rotors. That is because the existence of end plates prevents the air to escape from the buckets concave side to the external flow,

Department of Mechanical Engineering, Ferdowsi University of Mashhad, Mashhad, Iran

Corresponding author:
AR Teymourtash, Department of Mechanical Engineering, Ferdowsi University of Mashhad, Mashhad, Iran.
Email: Teymourtash@um.ac.ir

which would result in a higher pressure difference between the concave and convex sides of the buckets.

In order to reduce the fluctuations of the generated torque, Hayashi et al.[6–8] proposed and tested two-bucket rotors. Their results showed that the rotors with multiple stages can generate a smoother output torque without significant performance loss. Moreover, multi-stage rotors, which are mounted with a phase shift, eliminate the negative static torque of the Savonius rotors. Another possible solution to modify the starting characteristics of the Savonius rotors is using helically twisted blades instead of the semi-circular cylindrical buckets. Saha and Rajkumar[9] experimentally studied the twisted Savonius rotors with 0° to 25° twist angles. The results exhibited a relative increase of 27% in the power coefficient of the rotor with 15° twist, with respect to the zero-twist rotor. Kamoji et al.[10] performed experimental investigation on two-bladed helical Savonius rotors with 90° twist angle. It has been shown that a shaft-less helical Savonius rotor, with zero overlap ratio and 90° twist angle, having an aspect ratio of 0.88, has almost a same power coefficient as a conventional one with an aspect ratio of 1.0. However, the helical rotor takes advantage of the positive static torque in all rotor angles. Recently, Anbarsooz[11] performed numerical and experimental studies on the aerodynamic performance of helical Savonius rotors with 30° and 45° twist angles. Results showed that although the tested helical rotors have provided a more uniform time variations of the torque coefficient, the maximum power coefficient of the helical rotors were less than the conventional one. Irabu et al.[12] enhanced the performance of a Savonius rotor with about 50% increase in its power coefficient, using a guide-box tunnel with an area ratio of 0.43. Saha et al.[13] installed a semi-automatic valve in the blades of a Savonius rotor in a manner that, when the convex side of blade is on the windward side, the valve is open to reduce the blade negative torque. On the contrary, the valve is closed when the concave side of blade is on the windward side. Their experiments, using the new design, showed a 7% increase in the maximum power coefficient of the turbine, with respect to the rotor without the valves.

Burcin et al.[14,15] employed a curtain design in front of a Savonius rotor to guide the wind towards the concave side of the advancing blade and prevents the wind from reaching the convex side of the returning blade. The proposed arrangement prevents the production of negative torque by the returning blade and also accelerates the wind towards the concave side of the advancing blade. Using the curtain design, the power coefficient of the Savonius rotor increased considerably from 0.16 to 0.38. However, a main drawback of the curtain design and also the guide-box tunnel is that the Savonius turbine is no longer omnidirectional.

In this study, based on the patent presented by John Hunter (No. GB9524439.8),[16] a new design of the Savonius turbine is introduced, which keeps the omnidirectional characteristics of the Savonius rotor and at the same time, eliminates the negative torque of the returning blade. A schematic of the new design is depicted in Figure 1.

The blades are hinged to the drum and the negative torque of the returning blade is eliminated using opening/closing blades. The advancing blades are opened by the upcoming wind until they are held in the fully-opened position by stops. However, the returning blades are closed by the air flow and the wind flows over the drum with minimum resistance. A similar design has also been employed as a tidal current turbine by Yang and Lawn.[16] However, no investigations have been performed on the several geometrical parameters that might have significant effects on the turbine performance. Also, to the best knowledge of the authors, the current design have not yet been employed and tested for the wind energy production. In this study, the effects of the number of blades and the flow Reynolds number on the aerodynamic performance of the new turbine are investigated experimentally and numerically. The experiments are performed in an open jet type wind tunnel facility. However, for the numerical simulations, the multiple reference frame (MRF) approach, in conjunction with the SST k-ω turbulence model are employed, through ANSYS-Fluent 12.0 commercial software in a two-dimensional computational domain. It has been verified by D'Alessandro et al.[17] that, the end plates limit the three-dimensional flow behavior around the model tips. This fact allows comparing experimental results obtained on three-dimensional models to numerical data computed on two-dimensional domains. This is why there exist several studies on

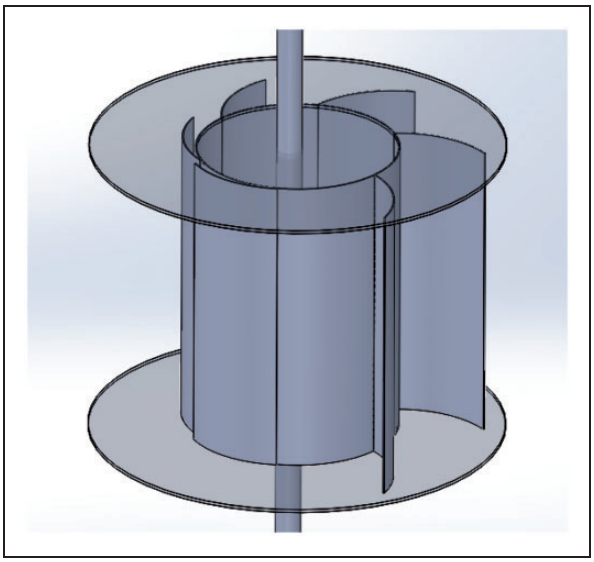

Figure 1. A schematic of the pivoted Savonius rotor with 6 blades.

vertical axis wind turbines, which are performed on two-dimensional computational domains.[18–21]

Rotor performance

A schematic of a 6-bladed rotor is depicted in Figure 2, where D is the drum diameter, R_c is the distance between the drum axis and the center of the fully opened blade chord, R_t is the distance between the drum axis and the tip of the fully-opened blade, and θ is the rotational angle, which is measured from the closest point of the drum to the incident flow and it determines the rotational angle of the trailing edge of a blade.

Each blade experiences two dynamic processes in one complete rotation, i.e. the opening and the closing processes. Yang and Lawn[16] experimentally determined the instances when these two processes are started and finished. Using a high-speed camera, instantaneous images of the turbine, running at various rotational speeds, were captured. Based on image processing, it was found that all the opening processes were started at about 90°, and finished at about 120°. Moreover, all the closing processes were started at about 180° and finished at about 360°. It was concluded that the opening and closing processes are almost independent of the tip speed ratio. Based on these findings, the blade positions in a cycle of rotation are determined for 6-bladed, 4-bladed, and 3-bladed rotors, which are shown in Figures 3 to 5. A cycle of rotation for a 6-bladed rotor is 60°; however, it is 90° and 120° for the 4-bladed and 3-bladed rotors, respectively.

Experimental setup

The experiments are performed in the low-speed open-jet type wind tunnel facility at Ferdowsi University of Mashhad, as shown in Figure 6. The wind tunnel test section is a $600 \times 600\,mm^2$ cylinder with a length of 2000 mm. However, the wind turbine assembly is placed 300 mm downstream of the tunnel exit. The wind speeds are accessible in the range of 0–25 m/s by varying the input voltage to the fan motor. The tested rotors with different number of blades (3, 4, and 6 blades) are shown in Figure 7. The turbines are made up of galvanized iron with a thickness of 0.4 mm. All the blades are pivoted on a cylindrical drum with 160 mm diameter. The geometrical parameters of the tested turbines are presented in Table 1.

Various mechanical loads are applied to the turbines through a pulley which is attached to the turbine shaft. A rope connects the pulley to two load cells. The accuracy of the load cells are ±1 N. The pulley and the shaft rotate simultaneously, while the rope is fixed and, as a result, a frictional force would be generated between the rope and the pulley. The frictional force is equal to the difference between the values of

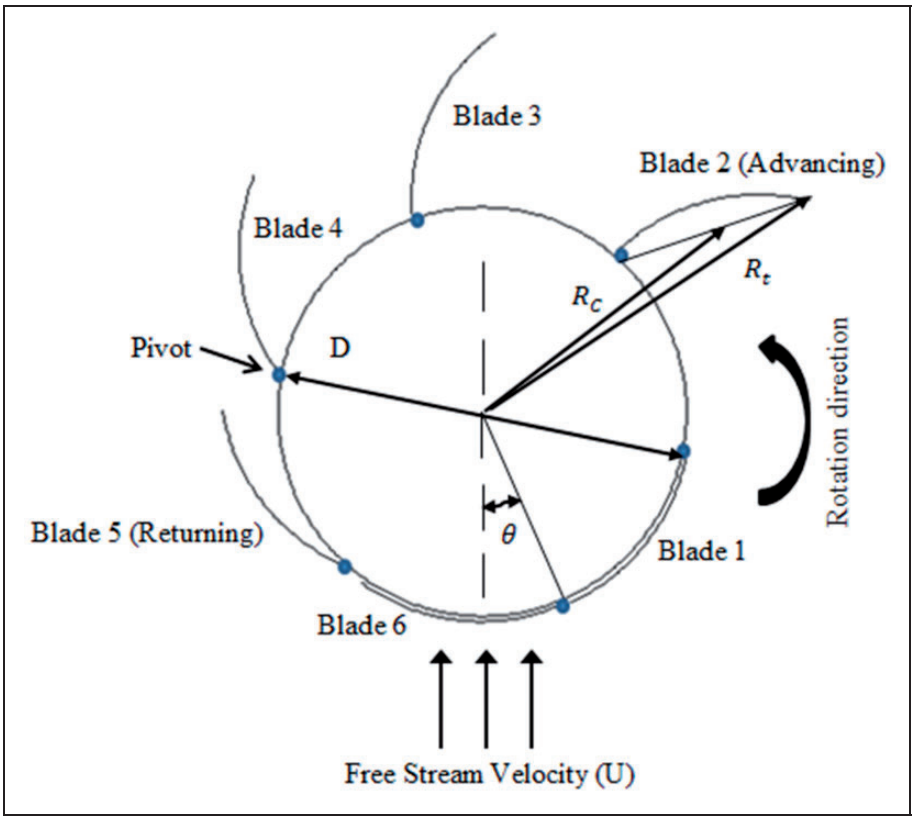

Figure 2. Rotor parameters.

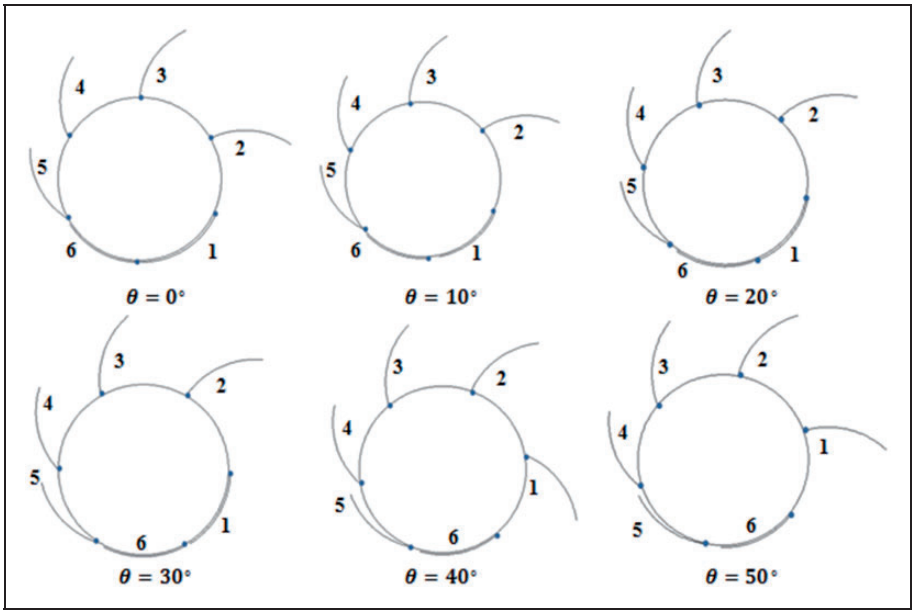

Figure 3. Blade positions in a cycle of rotation for the 6-bladed rotor.

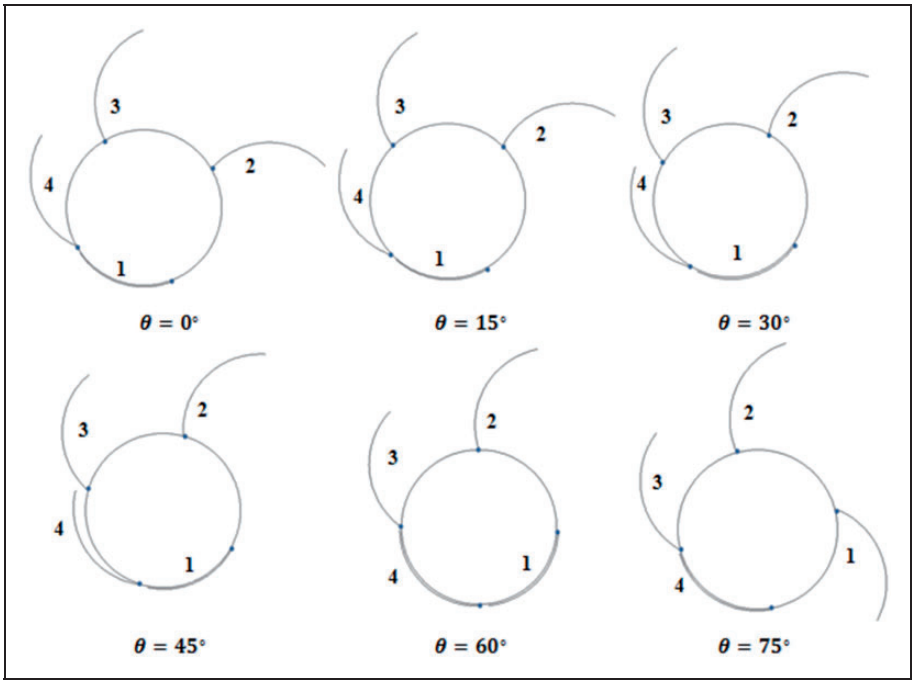

Figure 4. Blade positions in a cycle of rotation for the 4-bladed rotor.

the load cells. Multiplying this force by the radius of the pulley results the generated torque. A schematic of the pulley and load cells arrangement is depicted in Figure 8. The wind speed is measured by a blade anemometer (Lutron AM-4200) with an operating range of 0.8–30 m/s and an accuracy of 0.1 m/s. The rotational speed of the turbine is measured by an optical tachometer (Compact Instruments CT6/LSR) with an accuracy of 0.05% and operating range of 3–99,999 r/min.

All the experimental data were corrected to consider the blockage effects, based on the methodology proposed by Roy and Saha[22] and also used by Anbarsooz,[11] which was confirmed to be appropriate for open-jet type test sections.

The uncertainty analysis was carried out for all the experimental data, following the sequential perturbation technique suggested by Moffat.[23,24] The calculated maximum uncertainties in the main parameters are given in Table 2.

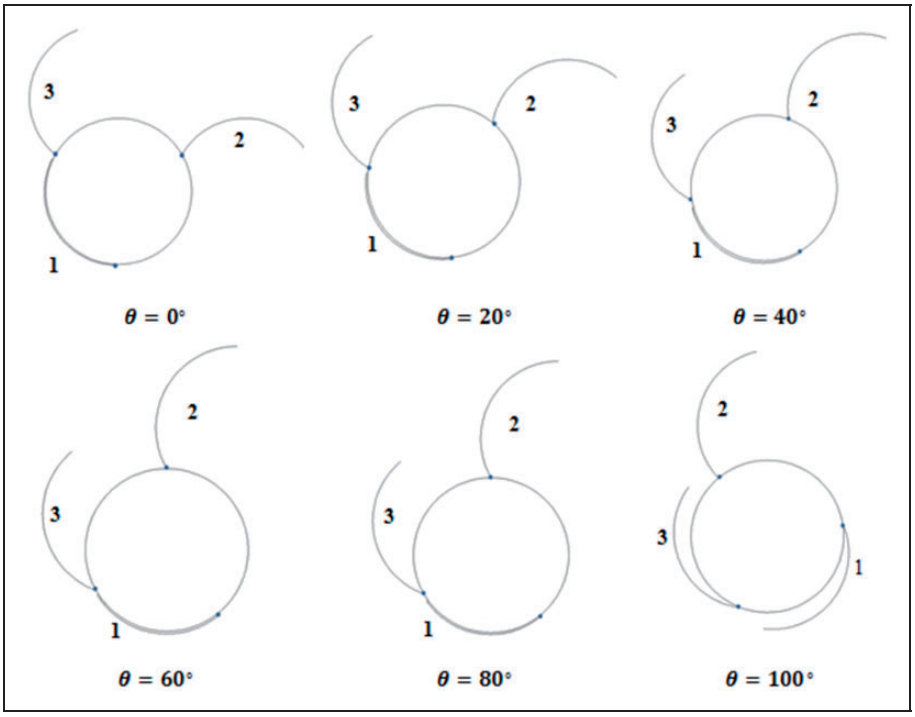

Figure 5. Blade positions in a cycle of rotation for the 3-bladed rotor.

Figure 6. Experimental setup at Ferdowsi University of Mashhad.

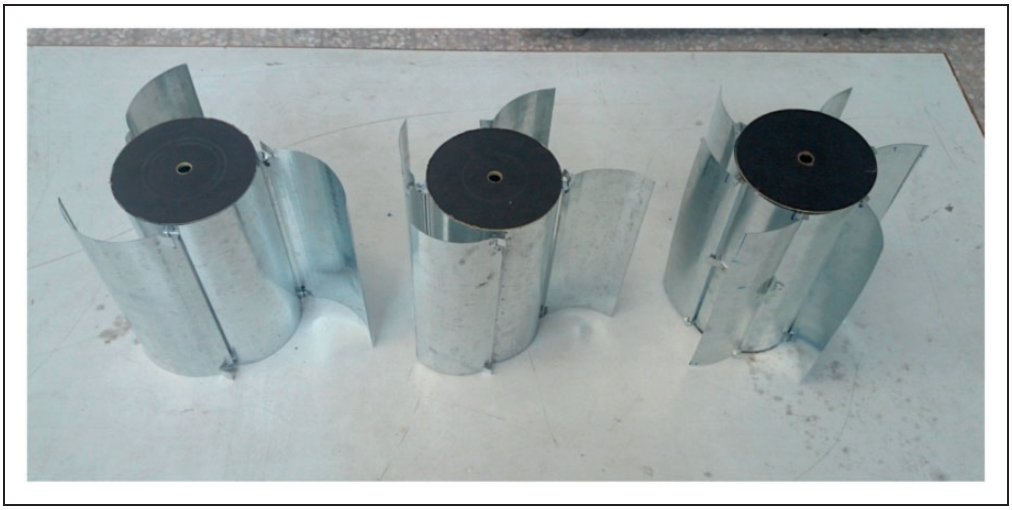

Figure 7. The rotors used for the experimental measurements of the current study.

Table 1. Geometrical parameters of the tested turbines.

Rotor type	D (mm)	H (mm)	R_c (mm)	R_t (mm)
3-bladed	160	320	144	211
4-bladed	160	320	135	193
6-bladed	160	320	120	160

Table 2. Uncertainties in various basic parameters.

Parameter uncertainty	(%)
Wind velocity	1.18
Diameter	0.18
Tip speed ratio	2.8
Torque coefficient	4.6
Power coefficient	5.1

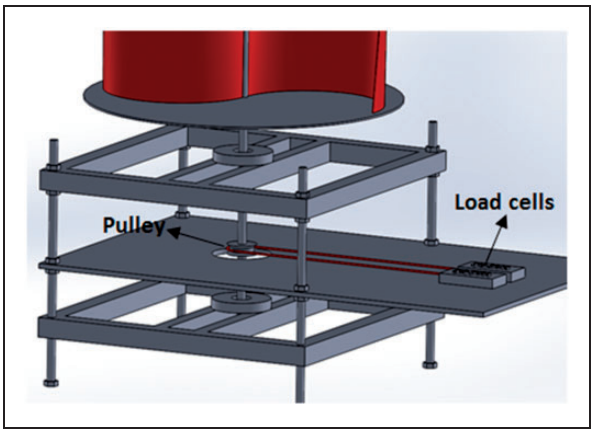

Figure 8. A schematic of the pulley and load cells arrangement.[11]

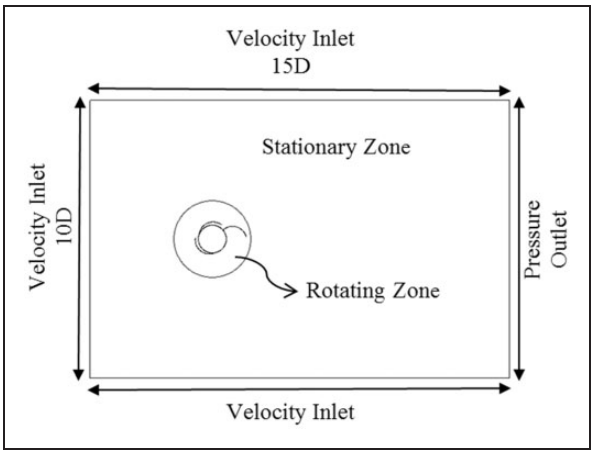

Figure 9. The computational domain and the boundary conditions.

Numerical procedure

The commercial software, ANSYS Fluent 12.0, is employed to perform the numerical simulations. In order to consider the effects of the turbine blades rotation on the flow field, the MRF model is used.[25] In the MRF formulation, the computational domain is divided into two subdomains, stationary and rotating, as shown in Figure 9. The size of the domain and the applied boundary conditions are also given on the figure. A constant rotational speed, $\vec{\omega}$, with respect to the stationary frame, can be applied to the rotating zone. The two-dimensional fluid flow governing equations, the conservation of mass and momentum, in the MRF model, are as follows[26]

$$\nabla \cdot \left(\rho \overrightarrow{v_r}\right) = 0 \tag{1}$$

$$\nabla \cdot \left(\rho \vec{v} \overrightarrow{v_r}\right) + \rho\left(\vec{\omega} \times \vec{v}\right) = -\nabla p + \nabla \cdot (\bar{\tau}) + \rho \vec{g} \tag{2}$$

where $\overrightarrow{v_r}$ is the relative velocity and $\vec{v}$ is the absolute velocity, defined as

$$\overrightarrow{v_r} = \vec{v} - \overrightarrow{u_r} \tag{3}$$

Here, $\overrightarrow{u_r}$ is the moving frame velocity. For the rotating zone of the current study, it can be written as

$$\overrightarrow{u_r} = \vec{\omega} \times \vec{r} \tag{4}$$

where $\vec{r}$ is the position vector, considered from the origin of the rotating frame.

The total moment vector, $\vec{M}_A$, about a specified center A, is computed by summing the cross products of the pressure and viscous force vectors ($\vec{F}_P$, $\vec{F}_v$) for each computational face with the position vector, $\vec{r}_{AB}$.

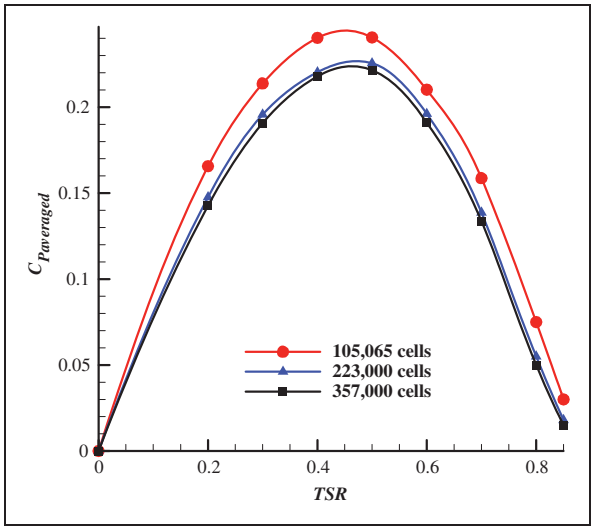

Figure 10. Grid resolution effects on the averaged power coefficient of the 3-bladed rotor.

The position vector is a vector from the specified moment center A to the force origin B[26]

$$\vec{M}_A = \vec{r}_{AB} \times \vec{F}_P + \vec{r}_{AB} \times \vec{F}_v \tag{5}$$

The terms in the above summation, represent the pressure and viscous moment vectors.

In this study, the SST k-ω turbulence model is used. The capability of this turbulence model in conjunction with the MRF model in simulating the aerodynamic performance of wind turbines has been confirmed by several researchers.[19,27]

A mesh study has been performed, in which, the size of the computational cells were gradually decreased until no noticeable changes in the generated power coefficient were observed. The effects of the grid size on the numerical power coefficients are depicted in Figure 10. The results suggested that an unstructured grid containing 223,000 cells is the most suitable grid in terms of both the numerical accuracy and computational cost. The final grid resolution near the turbine blades is shown in Figure 11. The value of y^+ depends on TSR, angular position of the rotor and number of the blades. For all of the simulations performed in this study, the value of y^+ has not exceeded 1.47. The rotating zone must contain the rotor at the fully-opened condition. In this study, the radius of the rotating zone is considered $1.05R_t$.

The boundary conditions for the turbulent equations at the inlet are a Turbulence Intensity = 1% and Turbulence Length Scale = 0.6 m. At the pressure outlet boundary, zero gradient for turbulent kinetic energy and specific dissipation rate are considered.

Results and discussion

The aerodynamic performance of the wind turbines can be expressed using two dimensionless coefficients,

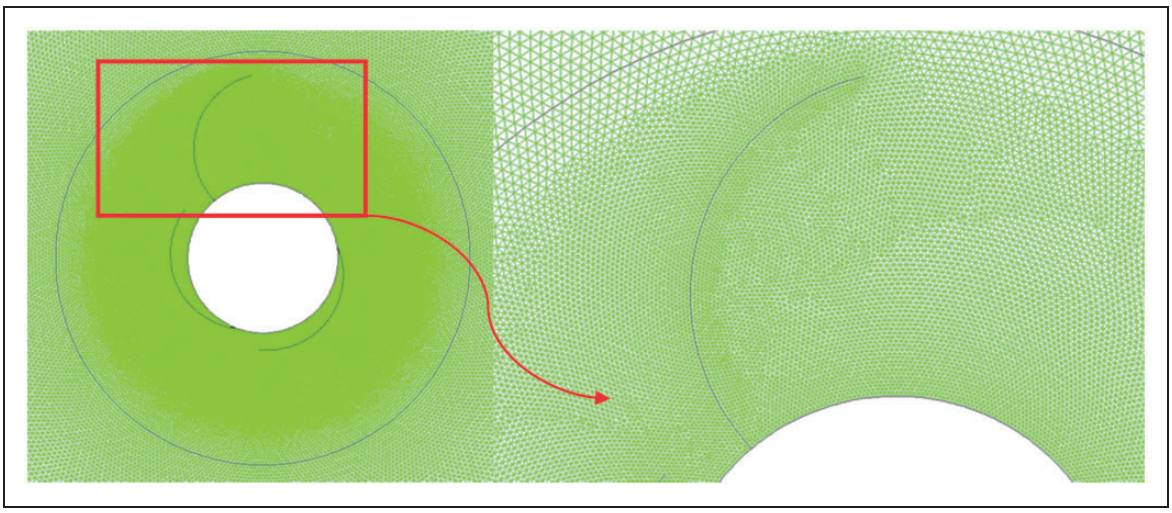

Figure 11. The computational grid near the turbine blades.

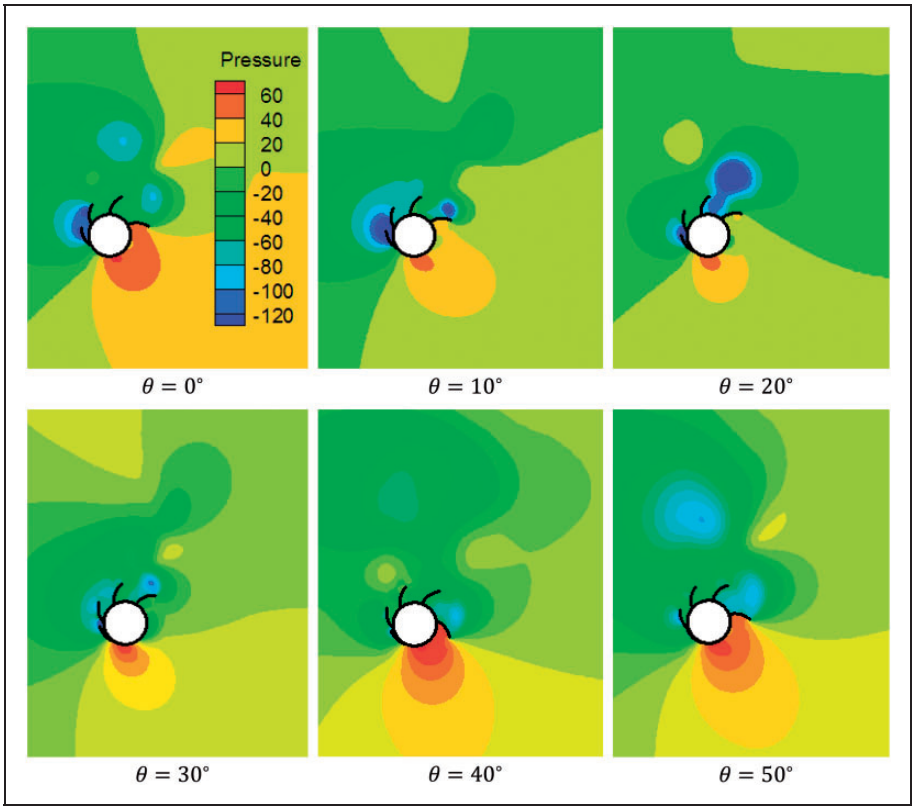

Figure 12. Pressure contours (Pascal) for the 6-bladed rotor at $TSR = 0.4$, for various rotor angular positions.

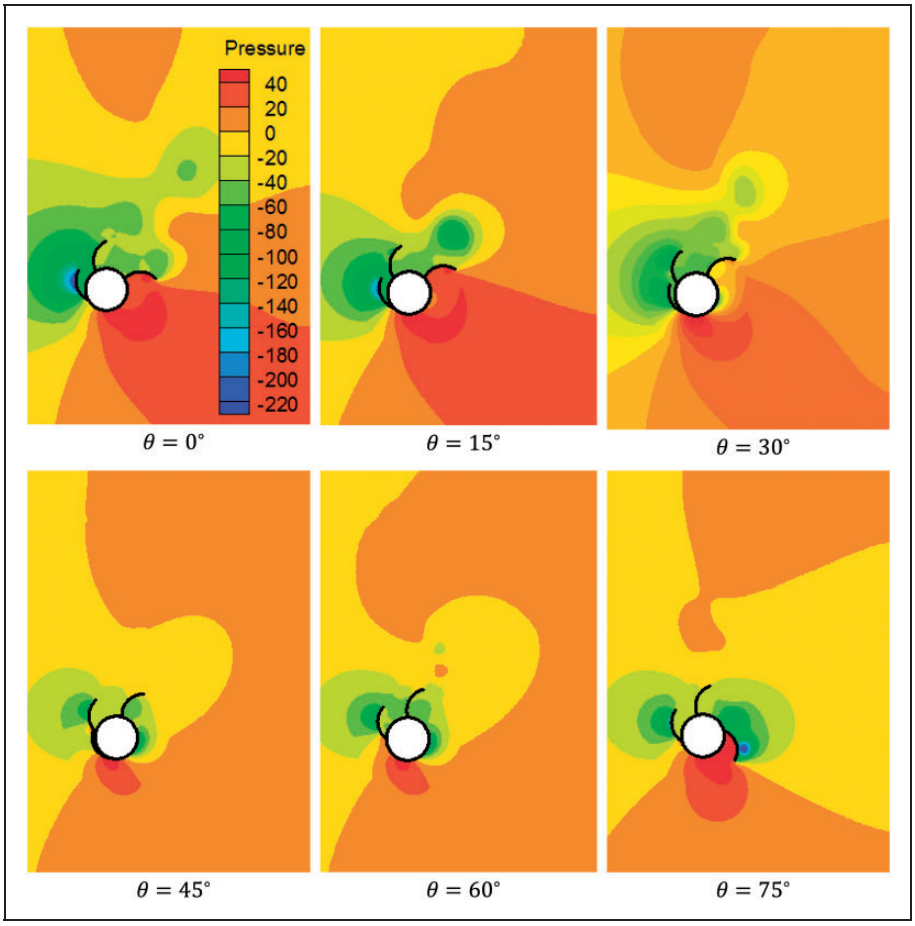

Figure 13. Pressure contours (Pascal) for the 4-bladed rotor at $TSR = 0.5$, for various rotor angular positions.

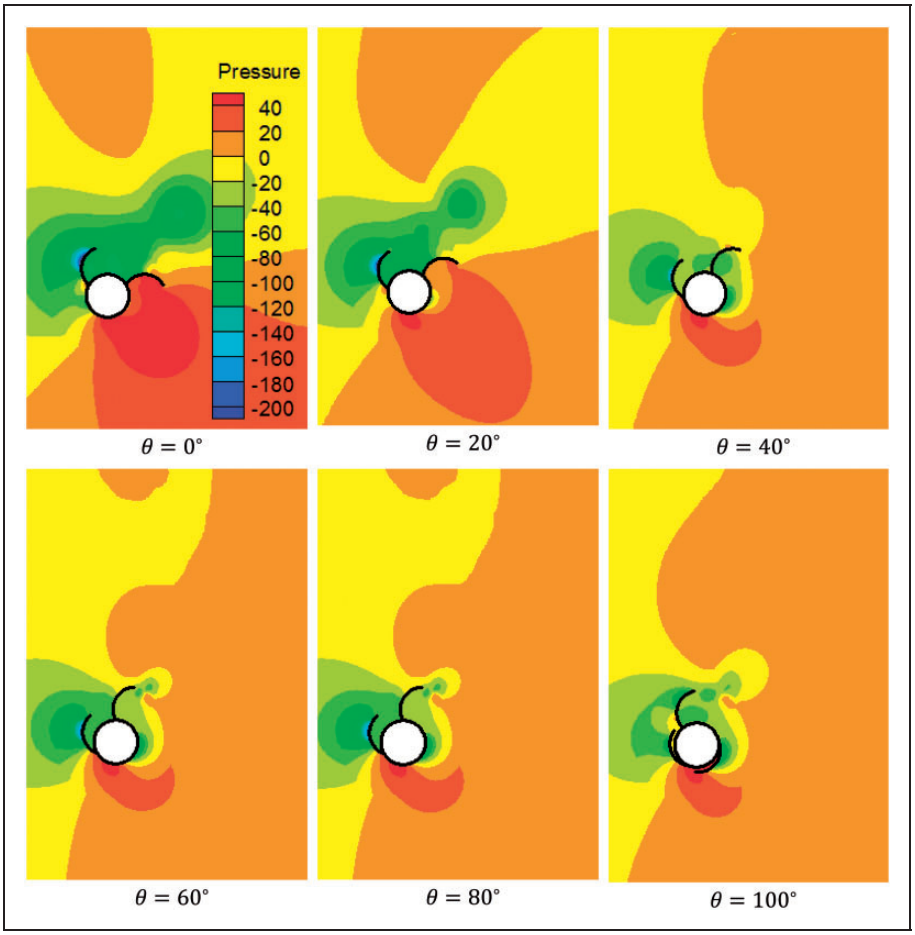

Figure 14. Pressure contours (Pascal) for the 3-bladed rotor at $TSR = 0.5$, for various rotor angular positions.

the power coefficient and the torque coefficient, as follows[16]

$$C_P = \frac{2T\omega}{\rho U^3 (R_t + D/2)H} \tag{6}$$

$$C_M = \frac{2T}{\rho U^2 (R_t + D/2)HR_c} \tag{7}$$

where T is the torque and ω is the rotational speed. The tip speed ratio, TSR, is defined as

$$TSR = \frac{\omega R_c}{U} \tag{8}$$

The power and torque coefficients could be correlated using TSR as

$$C_M = \frac{C_P}{TSR} \tag{9}$$

The flow Reynolds number, Re, is defined based on the drum diameter as

$$Re = \frac{\rho UD}{\mu} \tag{10}$$

where U is the free stream velocity and μ is the air viscosity.

The numerical pressure distributions around the 6-bladed rotor is depicted in Figure 12, for the air velocity of 9 m/s, corresponding to a Reynolds number of 9.9×10^4 based on the drum diameter. The 6-bladed rotor has six 60° cycles in one rotor revolution. The pressure contours are presented for six different angular positions of the rotor, in a cycle in one rotor revolution, at $TSR = 0.4$, which corresponds to the condition of maximum power coefficient of the rotors. At $\theta = 0°$, Blades 1 and 6 are fully closed and are lying on the cylindrical surface of the drum. Blades 2 and 3 are fully opened and Blades 4 and 5 are in the closing-process. Therefore, the only blades that contribute to the positive torque generation are Blades 2 and 3; however, Blade 2 has the main contribution as can be seen in the figure. As the angular position increases, at $\theta = 20°$, still Blades 1 and 6 are closed, while Blades 3, 4, and 5 are in the closing-process and the only blade in the fully-opened position is Blade 2. However, as shown in Figure 12, the pressure difference between the two surfaces of Blades 2 has decreased, which would lead to a decrease in the generated torque. At $\theta = 40°$, Blade 1 is in the opening-process. At this angular position, Blade 1 acts as

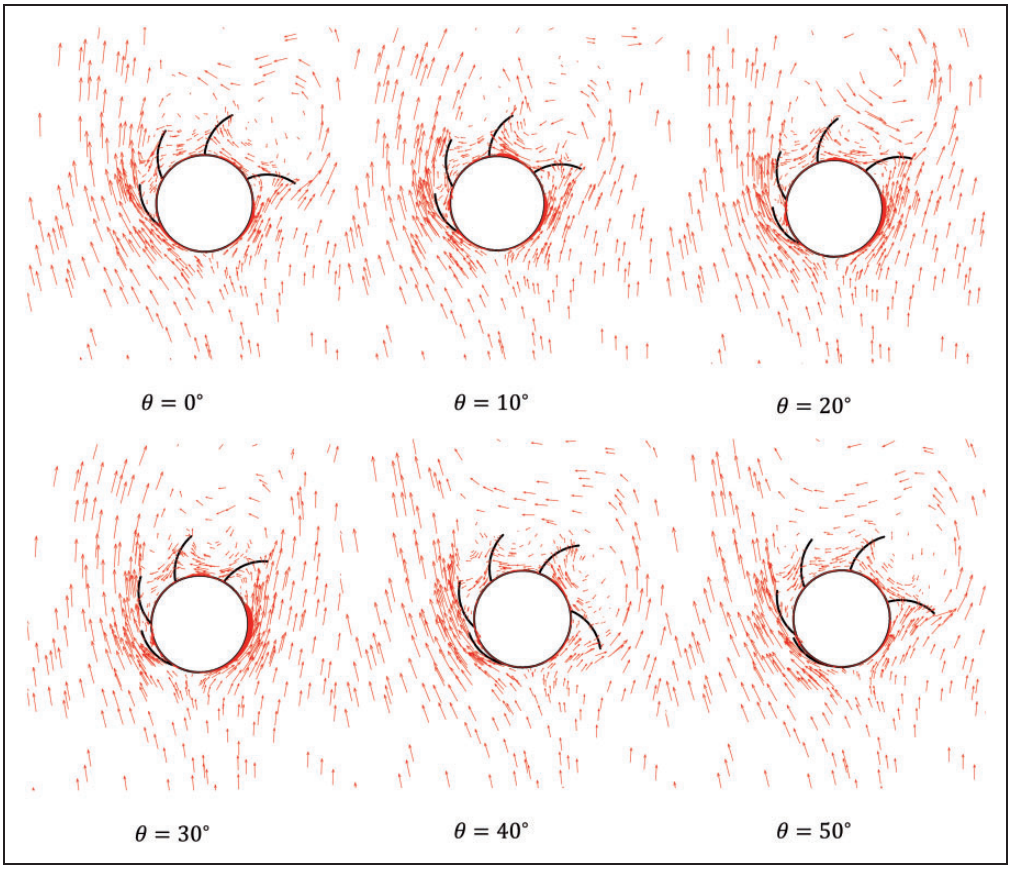

Figure 15. Velocity vector for the 6-bladed rotor at $TSR = 0.4$, for various rotor angular positions.

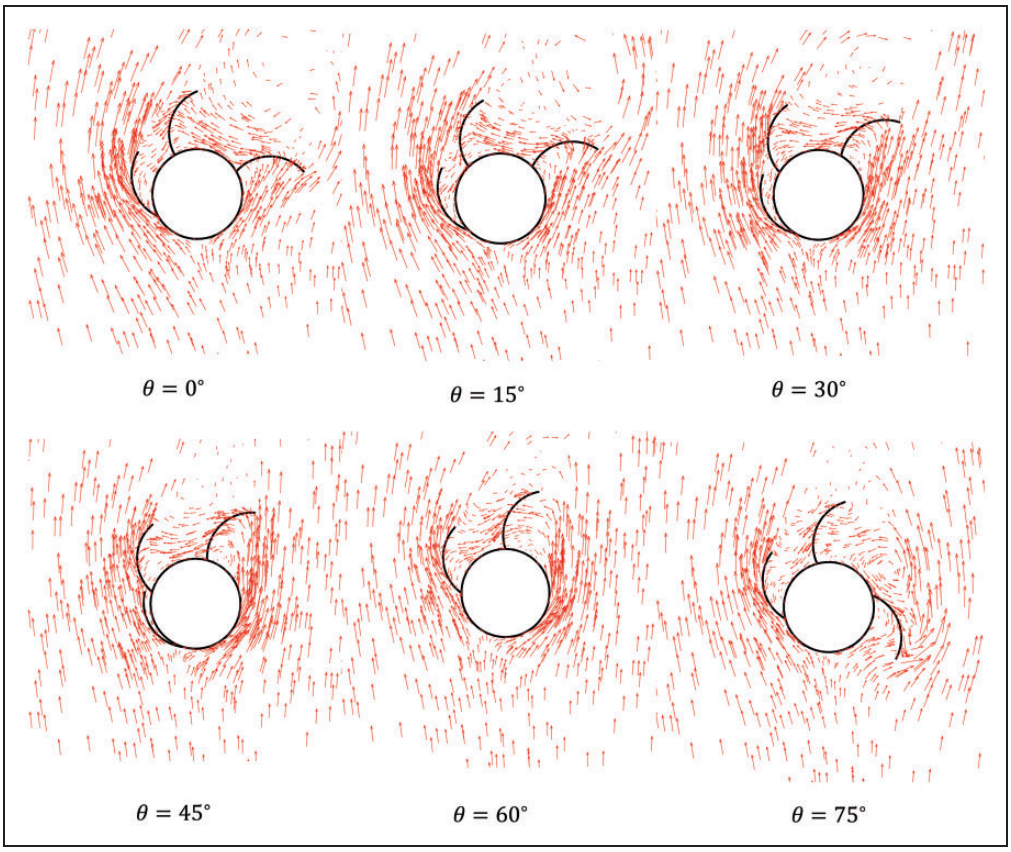

Figure 16. Velocity vector for the 4-bladed rotor at $TSR = 0.5$, for various rotor angular positions.

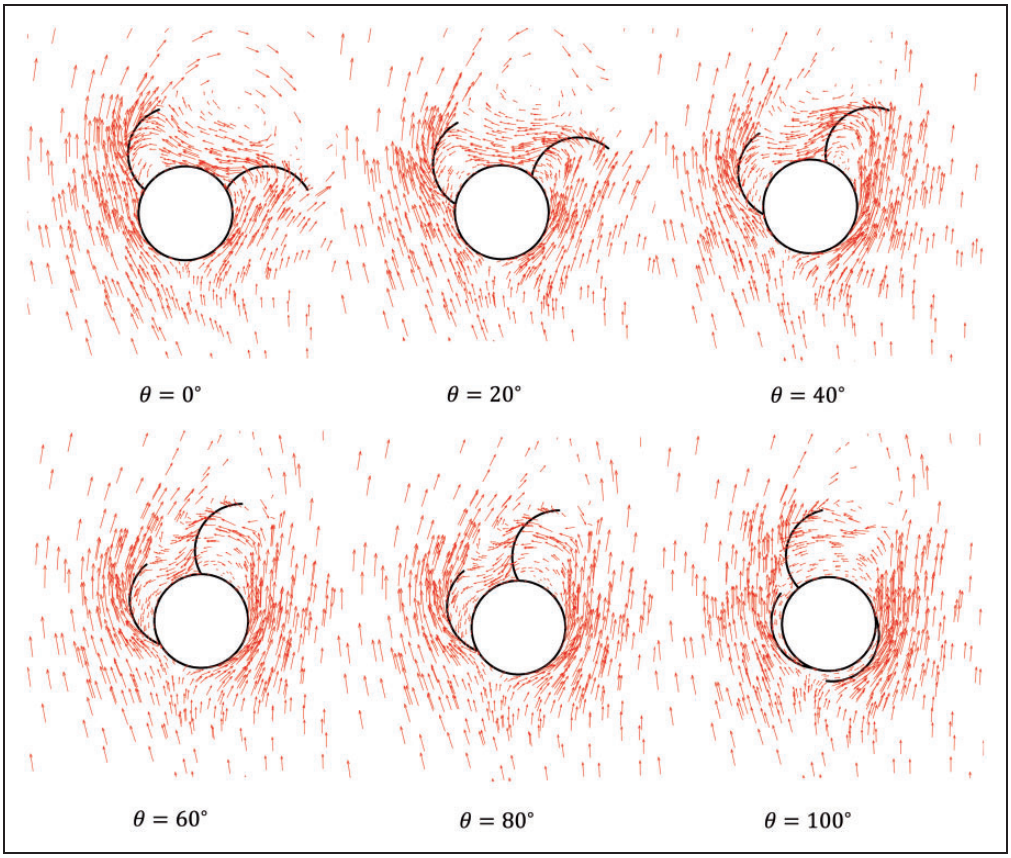

Figure 17. Velocity vector for the 3-bladed rotor at $TSR = 0.5$, for various rotor angular positions.

an obstacle which prevents the air from effectively reaching the fully opened Blade 2. In other words, Blade 2 is in the wake of Blade 1 and as a result, at this rotor angular position, the blade with maximum generated torque is Blade 1. It must be noted that the blades which are in the closing-process produce adverse pressure. Their contribution to the total torque is however not substantial (for the 6-bladed rotor at $TSR = 0.4$ and $\theta = 40^\circ$, the power coefficient of Blade 5, which is in the closing- process, is: -0.014.).

Similar pressure distributions are depicted for the 4-bladed and 3-bladed rotors in Figures 13 and 14, respectively. The 4-bladed and 3-bladed rotors have 90° and 120° cycles in one rotor revolution, respectively. As the number of blades decreases, with a same value of the drum diameter, the number of fully opened blades in one revolution decreases. However, the blades would be closer to a semicircular blade, which has a higher value of drag coefficient.[28]

The velocity vector distributions around the rotor blades at several angular positions are also illustrated in Figures 15, 16, 17 for the 6-, 4-, and 3-bladed rotors, respectively. The wake regions between the fully opened blade and the blade in the opening process can be well observed in these figures.

For a quantitative comparison between the torques generated by each blade, the torque coefficient of the blades which have considerable effects on the total torque, are plotted in Figure 18 at $TSR = 0.5$. For the 3-bladed rotor, in the $0^\circ < \theta < 80^\circ$, Blade 1 is closed and Blade 2 is fully-opened. In this angular range, it is only Blade 2 that is generating positive torque, until at $\theta > 80^\circ$, Blade 1 starts its opening process. At $\theta = 120^\circ$, Blade 2 is replaced by Blade 1 and the cycle would be repeated as explained above. The 4-bladed rotor has been also performed similarly; however, for the 6-bladed rotor, there are always two blades producing positive torque. The overall output torque coefficient of the rotors with various number of blades, in a full revolution are depicted in Figure 19.

As shown in Figure 18, the output torque oscillations are decreased, as the number of blades increases. In other words, increasing the number of blades would result in a smoother torque generation of the turbine. Nevertheless, as the number of blades increases, the minimum values of the torque coefficients are not changed considerably, but the maximum values are decreased. This figure also reveals that the proposed rotor has no negative total torque coefficient in a revolution, which is the main advantage of these rotors.

The total averaged torque coefficients as a function of TSR is plotted in Figure 20 for the rotors with different number of blades. In this figure, the numerical results are also compared with the experimental data. As shown in the figure, the numerical and

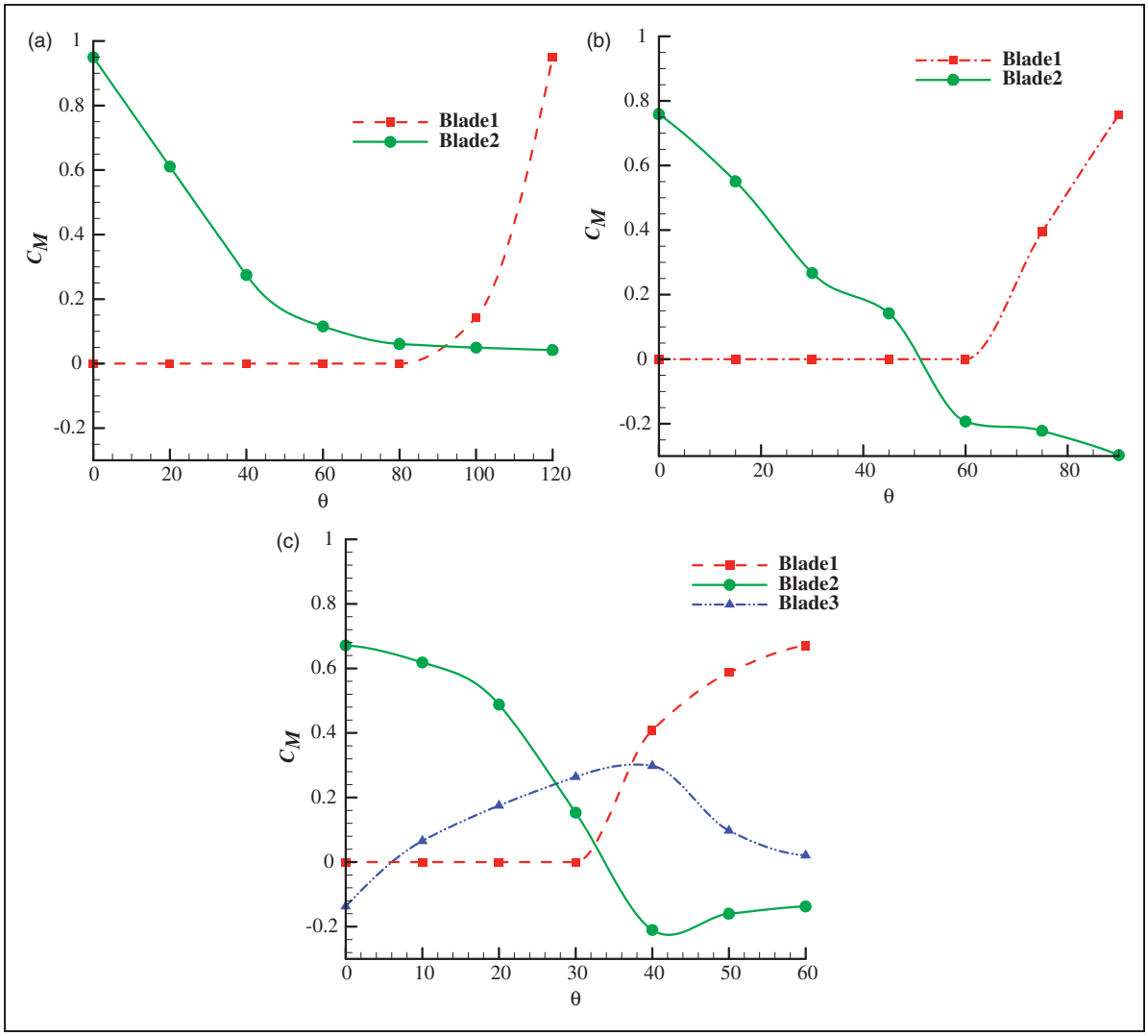

Figure 18. Evolution of the numerical torque coefficients developed by the rotor blades at $TSR = 0.5$: (a) rotor with 3 blades; (b) rotor with 4 blades; (c) rotor with 6 blades.

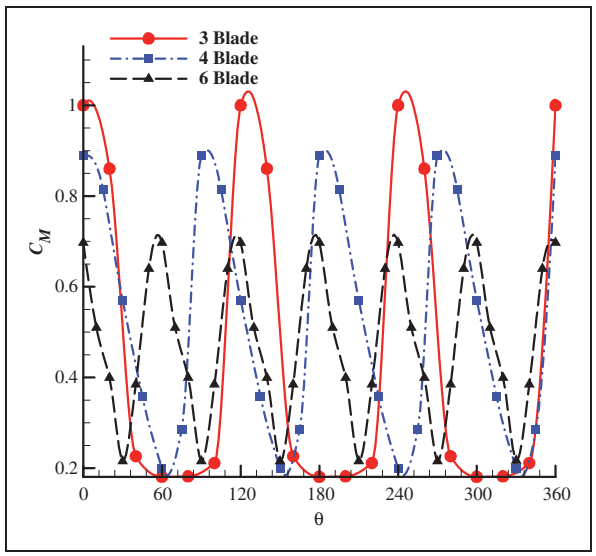

Figure 19. The variations of the numerical total torque coefficients, for the rotors with various number of blades, in one complete rotor revolution at $TSR = 0.4$.

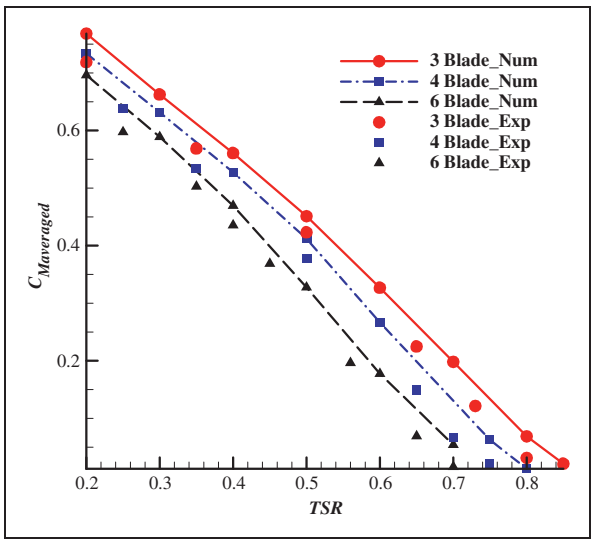

Figure 20. Numerical averaged torque coefficients, $C_{M\_averaged}$, as a function of TSR, in comparison with the experimental data for the rotors with different number of blades.

experimental results are in a convincing agreement, which validates the employed numerical methodology.

As the *TSR* decreases, the relative velocity between the wind and the advancing blade decreases. This would lead to a higher pressure on the blade and as a result, the torque coefficient increases. Figure 20 also demonstrates that the 3-bladed rotor has a higher value of torque coefficient in all the *TSR*s, in comparison with the 4-bladed and 6-bladed rotors. As explained above, the reason for this behavior is that as the number of blades increases, each advancing blade would deflect the air from reaching the next advancing blade, effectively. This behavior has also been observed in the traditional Savonius rotors which is referred to as the "cascade effect".[28]

The numerical results for the power coefficient as a function of *TSR* are compared with the experimental data in Figure 21, for the rotors with different number of blades, where a good agreement can be observed.

As shown in Figure 21, both the maximum $C_{p\text{-}averaged}$ and its corresponding *TSR* increase, as the number of blades decreases. Furthermore, the operating range of *TSR* is larger for the 3-bladed rotor in comparison with the 4-bladed and 6-bladed rotors. The values of the operating range of rotors (based on *TSR*) and also the points of maximum power coefficients are given in Table 3. In this table, the numerical results are also compared with the experimental data. The error between the numerical results might be due to the two-dimensional assumption for the numerical simulations and neglecting the effects of tip vortices at the endplates. Although the bearings are carefully designed to have minimum friction, some errors might be due to the small frictions in the bearings, which are inevitable.

The effects of the Reynolds number on the aerodynamic performance of the 3-bladed rotor are also investigated numerically and experimentally. The investigations are performed at three Reynolds numbers of 7.7×10^4, 9.9×10^4, and 1.2×10^5 corresponding to the wind speeds of 7.0, 9.0, and 11.0 m/s, and the results are presented in Figure 22. The figure shows that the Reynolds number does not have significant effects on the average power coefficient of the rotor, in the studied range of Reynolds numbers. Increasing the Reynolds number from 7.7×10^4 to 1.2×10^5 have increased the maximum power coefficient

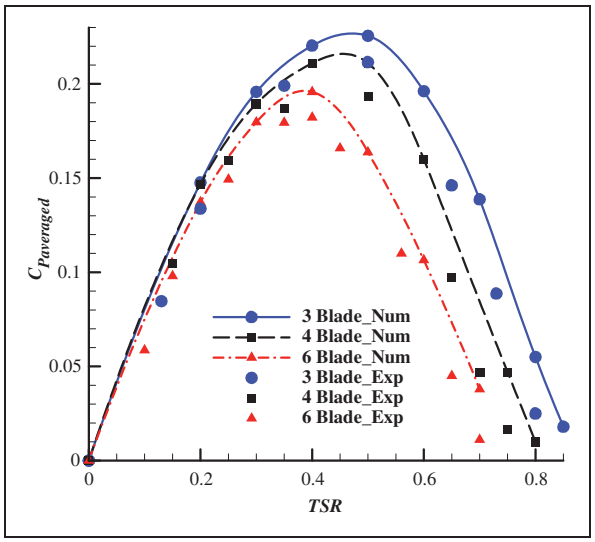

Figure 21. Comparison of the numerical averaged power coefficients, $C_{P\_averaged}$, with the experimental data, for the rotors with different number of blades.

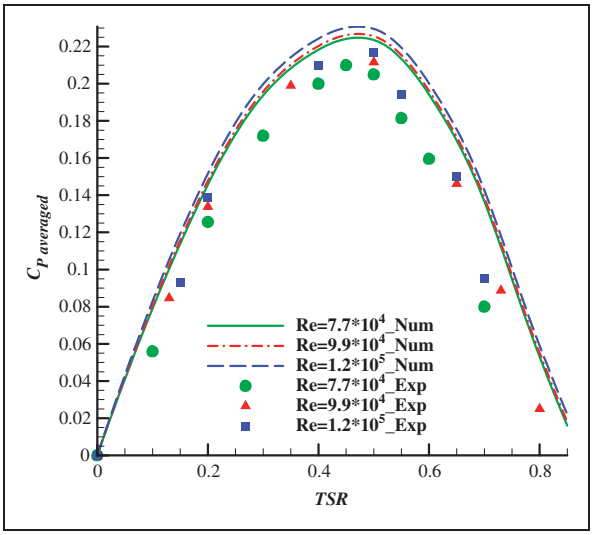

Figure 22. Comparison of the numerical averaged power coefficients, $C_{P\_averaged}$, with the experimental data, for the 3-bladed rotor at various Reynolds numbers.

Table 3. The experimental and numerical operating ranges and the points of maximum power coefficient, for the rotors with different number of blades.

	Maximum $C_{p\text{-}averaged}$			*TSR* corresponding to the maximum $C_{p\text{-}averaged}$		Operating range of *TSR*	
Rotor type	Num.	Exp.	Error (%)	Num.	Exp.	Num.	Exp.
6-bladed	0.195	0.18	8.33	0.4	0.4	0–0.75	0–0.7
4-bladed	0.211	0.19	11.05	0.5	0.5	0–0.8	0–0.75
3-bladed	0.225	0.21	7.14	0.5	0.5	0–0.85	0–0.8

2.68 % in the numerical simulations and 3.19% in the experiments.

Conclusion

In order to eliminate the negative torque of the returning blades of the Savonius rotor, a recently introduced design has suggested pivoted blades, which might be a promising solution. In this study, the aerodynamic performance of the newly proposed turbine has been investigated, using experimental wind-tunnel measurements and numerical simulations. The experimental measurements are performed in a subsonic open-jet type wind tunnel facility at Ferdowsi University of Mashhad. The numerical simulations are performed using the Ansys-Fluent commercial software, using the MRF model in conjunction with the SST k-ω turbulence model. The numerical results are in a convincing agreement with the experimental data with less than 12% relative error. The investigations are carried out on rotors with three different number of blades, i.e. 3, 4, and 6 blades, at several Reynolds numbers. The most significant findings of the current study can be summarized as:

- ✓ The new rotor has no negative torque in one complete revolution and the 3-bladed rotor has the best aerodynamic performance, in a manner that, it reaches a maximum power coefficient of 0.21 at $TSR = 0.5$.
- ✓ Although increasing the number of blades decreases the output torque oscillations, it decreases the average power coefficient of the rotor, due to a cascade effect.
- ✓ Both the maximum $C_{p\text{-}averaged}$ and its corresponding TSR increase, as the number of blades decreases.
- ✓ The operating range of TSR is larger for the 3-bladed rotor in comparison with the 4-bladed and 6-bladed rotors.
- ✓ In the studied range of Reynolds numbers, $7.7 \times 10^4 \leqslant Re \leqslant 1.2 \times 10^5$, the Reynolds number does not have significant effects on the average power coefficients of the rotors.

Declaration of Conflicting Interests

The author(s) declared no potential conflicts of interest with respect to the research, authorship, and/or publication of this article.

Funding

The author(s) received no financial support for the research, authorship, and/or publication of this article.

References

1. TangZP, Yao YX, Zhou L, et al. A review on the new structure of Savonius wind turbines. *Adv Mater Res* 2013; 608–609: 467–478.
2. Duffett I, Perry J, Stockwood B, et al. Design and evaluation of twisted Savonius wind turbine. 2009.
3. Fujisawa N. On the torque mechanism of Savonius rotors. *J Wind Eng Ind Aerodyn* 1992; 40: 277–292.
4. Kianifar A and Anbarsooz M. Blade curve influences on the performance of Savonius rotors: Experimental and numerical. *Proc IMechE, Part A: J Power and Energy* 2011; 225: 343–350.
5. Alexander AJ and Holownia BP. Wind tunnel tests on a Savonius rotor. *J Wind Eng Ind Aerodyn* 1978; 3: 343–351.
6. Hayashi T, Li Y, Hara Y, et al. Wind tunnel tests on a different phase three-stage Savonius rotor. *JSME Int J Ser B Fluids Therm Eng* 2005; 48: 9–16.
7. Kamoji MA, Kedare SB and Prabhu SV. Experimental investigations on single stage modified Savonius rotor. *Appl Energy* 2009; 86: 1064–1073.
8. Gupta R, Biswas A and Sharma KK. Comparative study of a three-bucket Savonius rotor with a combined three-bucket Savonius–three-bladed Darrieus rotor. *Renew Energy* 2008; 33: 1974–1981.
9. Saha UK and Rajkumar MJ. On the performance analysis of Savonius rotor with twisted blades. *Renew Energy* 2006; 31: 1776–1788.
10. Kamoji MA, Kedare SB and Prabhu SV. Performance tests on helical Savonius rotors. *Renew Energy* 2009; 34: 521–529.
11. Anbarsooz M. Aerodynamic performance of helical Savonius wind rotors with 30° and 45° twist angles: Experimental and numerical studies. *Proc IMechE, Part A: J Power and Energy* 2016.
12. Irabu K and Roy JN. Characteristics of wind power on Savonius rotor using a guide-box tunnel. *Exp Therm Fluid Sci* 2007; 32: 580–586.
13. Saha UK, Thotla S and Maity D. Optimum design configuration of Savonius rotor through wind tunnel experiments. *J Wind Eng Ind Aerodyn* 2008; 96: 1359–1375.
14. Altan BD and Atılgan M. The use of a curtain design to increase the performance level of a Savonius wind rotors. *Renew Energy* 2010; 35: 821–829.
15. Tartuferi M, D'Alessandro V, Montelpare S, et al. Enhancement of Savonius wind rotor aerodynamic performance: A computational study of new blade shapes and curtain systems. *Energy* 2015; 79: 371–384.
16. Yang B and Lawn C. Fluid dynamic performance of a vertical axis turbine for tidal currents. *Renew Energy* 2011; 36: 3355–3366.
17. D'Alessandro V, Montelpare S, Ricci R, et al. Unsteady aerodynamics of a Savonius wind rotor: A new computational approach for the simulation of energy performance. *Energy* 2010; 35: 3349–3363.
18. Nasef MH, El-Askary WA, AbdEl-hamid AA, et al. Evaluation of Savonius rotor performance: Static and dynamic studies. *J Wind Eng Ind Aerodyn* 2013; 123: 1–11.
19. El-Askary WA, Nasef MH, AbdEl-hamid AA, et al. Harvesting wind energy for improving performance of Savonius rotor. *J Wind Eng Ind Aerodyn* 2015; 139: 8–15.
20. Emmanuel B and Jun W. Numerical study of a six-bladed savonius wind turbine. *J Solar Energy Eng* 2011; 133: 044503–044503.
21. Torresi M, Fortunato B, Pascazio G, et al. CFD analysis of a Savonius rotor in a confined test section and in

open field, volume 1: Aircraft engine; ceramics; coal, biomass and alternative fuels. *Wind Turbine Technol* 2011.
22. Roy S and Saha UK. Wind tunnel experiments of a newly developed two-bladed Savonius-style wind turbine. *Appl Energy* 2015; 137: 117–125.
23. Moffat RJ. Contributions to the theory of single-sample uncertainty analysis. *J Fluids Eng* 1982; 104: 250–258.
24. Moffat RJ. Describing the uncertainties in experimental results. *Exp Therm Fluid Sci* 1988; 1: 3–17.
25. Pope K, Rodrigues V, Doyle R, et al. Effects of stator vanes on power coefficients of a zephyr vertical axis wind turbine. *Renew Energy* 2010; 35: 1043–1051.
26. Ansys Inc. *ANSYS Fluent 12.0 theory guide*. Canonsburg, PA: ANSYS, Inc., 2009.
27. Lanzafame R, Mauro S and Messina M. Wind turbine CFD modeling using a correlation-based transitional model. *Renew Energy* 2013; 52: 31–39.
28. Akwa JV, Vielmo HA and Petry AP. A review on the performance of Savonius wind turbines. *Renew Sustain Energy Rev* 2012; 16: 3054–3064.

Appendix

Notation

C_P	power coefficient
C_M	torque coefficient
D	drum diameter
$\vec{F}_P$	pressure force vector
$\vec{F}_v$	viscos force vector
H	drum height
$\vec{M}_A$	total moment vector
p	pressure
r	position vector
$\vec{r}_{AB}$	position vector
R_c	distance between the drum axis and the center of the fully-opened blade chord
R_t	distance between the drum axis and the tip of the fully-opened blade
Re	Reynolds number
T	torque
TSR	tip speed ratio
u_r	moving frame velocity
U	freestream velocity
μ	air viscosity
ω	rotational speed
ρ	air density
$\bar{\tau}$	stress tensor
θ	rotational angle
υ	absolute velocity
υ_r	relative velocity